Article

Dependence of Transition State Structure on Substrate: The Intrinsic C-13 Kinetic Isotope Effect Is Different for Physiological and Slow Substrates of the Ornithine Decarboxylase Reaction Because of Different Hydrogen Bonding Structures

Daria Sicinska, Donald G. Truhlar, and Piotr Paneth

J. Am. Chem. Soc., **2005**, 127 (15), 5414-5422• DOI: 10.1021/ja042298p • Publication Date (Web): 19 March 2005

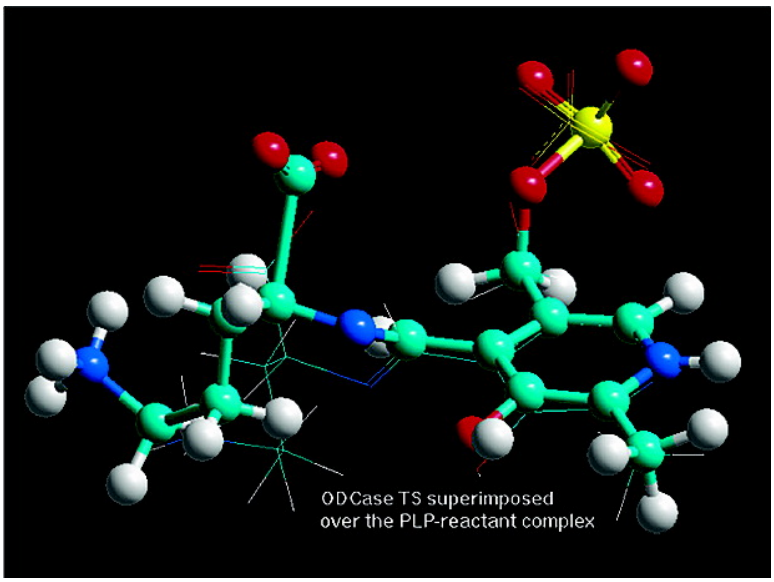

More About This Article

Additional resources and features associated with this article are available within the HTML version:

- Supporting Information
- Links to the 3 articles that cite this article, as of the time of this article download
- Access to high resolution figures
- Links to articles and content related to this article
- Copyright permission to reproduce figures and/or text from this article

View the Full Text HTML

J|A|C|S
ARTICLES
Published on Web 03/19/2005

Dependence of Transition State Structure on Substrate: The Intrinsic C-13 Kinetic Isotope Effect Is Different for Physiological and Slow Substrates of the Ornithine Decarboxylase Reaction Because of Different Hydrogen Bonding Structures

Daria Sicinska,[†] Donald G. Truhlar,*[,‡] and Piotr Paneth*[,†]

Contribution from the Institute of Applied Radiation Chemistry, Technical University of Lodz, Zeromskiego 116, 90-924 Lodz, Poland, and Department of Chemistry and Supercomputing Institute, University of Minnesota, Minneapolis, Minnesota 55455-0431

Received December 22, 2004; E-mail: truhlar@umn.edu; paneth@p.lodz.pl

Abstract: Ornithine decarboxylase is the first and the rate-controlling enzyme in polyamine biosynthesis; it decarboxylates L-ornithine to form the diamine putrescine. We present calculations performed using a combined quantum mechanical and molecular mechanical (QM/MM) method with the AM1 semiempirical Hamiltonian for the wild-type ornithine decarboxylase reaction with ornithine (the physiological substrate) and lysine (a "slow" substrate) and for mutant E274A with ornithine substrate. The dynamical method is variational transition state theory with quantized vibrations. We employ a single reaction coordinate equal to the carbon−carbon distance of the dissociating bond, and we find a large difference between the intrinsic kinetic isotope effect for the physiological substrate, which equals 1.04, and that for the slow substrate, which equals 1.06. This shows that, contrary to a commonly accepted assumption, kinetic isotope effects on slow substrates are not always good models of intrinsic kinetic isotope effects on physiological substrates. Furthermore, analysis of free-energy-based samples of transition state structures shows that the differences in kinetic isotope effects may be traced to different numbers of hydrogen bonds at the different transition states of the different reactions.

Introduction

Kinetic isotope effects (KIEs) are a very sensitive tool for elucidating mechanisms of chemical and enzymatic reactions and for inferring transition state structure. Because carbon dioxide is especially amenable to convenient isotopic analysis of its carbon content, ^{13}C KIEs have been widely used in studies of spontaneous and enzymatic decarboxylation reactions.[1,2] The enzymatic processes, however, are always complex reactions involving more than one step. Even when the chemical step in an enzymatic reaction is the only isotopically sensitive step, the observed kinetic isotope effect (KIE_{obs}) may be different from the KIE for the chemical step, which is called the intrinsic KIE.

When KIEs are measured by competition, they provide mechanistic information only for steps up to and including the first irreversible step, and the extent to which they reflect the chemical step depends on all the rate constants in the mechanism up to this step. This can be illustrated by considering the simplest enzymatic reaction that includes a reversible binding step. Such a reaction is characterized by two rate constants k_1 and k_2 corresponding to forward and reverse binding steps and a third rate constant k_3 corresponding to an irreversible chemical conversion step:

$$E + S \underset{k_2}{\overset{k_1}{\rightleftharpoons}} ES \xrightarrow{k_3} E + P \qquad (1)$$

If only the chemical step is isotope-sensitive, then the steady-state approximation gives

$$KIE_{obs} = \frac{KIE_3 + C}{1 + C} \qquad (2)$$

where the parameter C equals k_3/k_2 and is called the commitment to catalysis, and where KIE_3 corresponds to the kinetic isotope effect on the chemical rate constant k_3 and is called the intrinsic KIE. It can be seen from eq 2 that the observed KIE depends not only on the intrinsic one but also on the ratio k_3/k_2. When this ratio approaches zero, KIE_{obs} approaches KIE_3. When it is much larger than unity, KIE_{obs} approaches unity.[3]

Carbon-13 KIEs have frequently been used to evaluate relative values of rate constants in enzymatic mechanisms. For this purpose, the observed value (KIE_{obs}) was compared with the intrinsic one (KIE_3), and the ratio k_3/k_2 was obtained, or—

[†] Technical University of Lodz.
[‡] University of Minnesota.

(1) O'Leary, M. H. Heavy-Atom Isotope Effects in Enzyme-Catalyzed Reaction. In *Stable Isotopes*; Schmidt, H. L., Förstel, H., Heinzinger, K., Eds.; Elsevier: Amsterdam, 1982; p 67.
(2) O'Leary, M. H. *Acc. Chem. Res.* **1988**, *21*, 450.
(3) Cleland, W. W., O'Leary, M. H., Northrop, D. B., Eds.; *Isotope Effects on Enzyme-Catalyzed Reactions*; University Park Press: Baltimore, MD, 1977.

10.1021/ja042298p CCC: $30.25

for more complicated mechanisms—inferences about partially rate-limiting steps prior to the chemical step were drawn. To be able to carry out such an analysis, KIE_3 has to be evaluated. This can be done in several ways.[4] In the case of a multisubstrate sequential reaction, changing the concentration of one of the reactants, frequently together with changes of reaction conditions (e.g., temperature, pH), can yield the intrinsic isotope effect. This approach was demonstrated in the case of orotidine decarboxylase.[5] The other approach is to use an alternative reactant ("slow" substrate). The philosophy behind this method is that for many substrates that react slowly, $k_3 \ll k_2$, and the commitment effectively approaches zero; thus the observed KIE approaches the intrinsic effect, and one sometimes hypothesizes that this is the same as the intrinsic KIE for the physiological substrate. A similar approach relies on the use of an appropriately mutated enzyme to slow the reaction. Although the slow-substrate and mutated-enzyme hypotheses[6,7] have been widely invoked, sometimes justified as reasonable, and sometimes questioned, the precise limits of their validity are unknown, and examples of *how* they might fail (if and when they do fail) would be very instructive.

Ornithine decarboxylase (ODC, EC 4.1.1.17) is a good case for testing these procedures since experimental values of carbon kinetic isotope effects on the ornithine decarboxylase reaction and several of its active-site mutants have been already reported,[7] and the 3D structure of this enzyme is available[8] for use in building rational theoretical models. We will calculate KIEs for the wild-type enzyme with the physiological substrate, ornithine, and with a slow substrate, lysine, and also for the E274A mutant with ornithine. The E274A mutant substitutes alanine for Glu274, a strictly conserved residue that enhances the electron-withdrawing character of the pyridoxal 5′-phosphate (PLP) ring by interacting with its protonated pyridine nitrogen.[9]

Ornithine decarboxylase is a lyase that catalyzes the decarboxylation of ornithine to produce putrescine (1,4-diaminobutane), leading eventually to higher polyamines that are essential for cell growth, differentiation, and division. Wild-type ornithine decarboxylase catalyzes conversion of the L isoform of ornithine.[10−12] It can also act on L-lysine and very inefficiently on arginine,[10,13] but these reactions are not significant for cellular metabolism. ODC requires PLP as a cofactor, which is bound to the active-site residue Lys69 by a Schiff-base linkage.

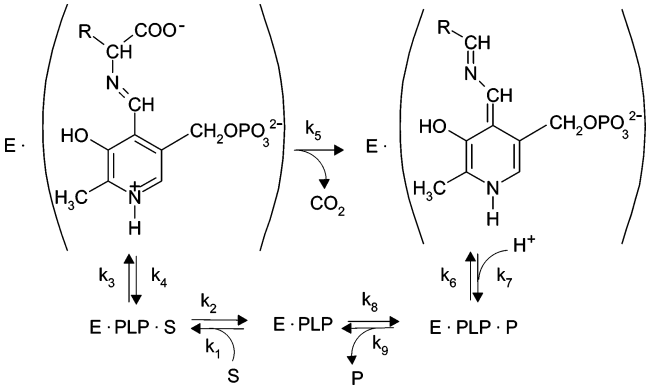

Figure 1. Reaction cycle catalyzed by ODC.

Active mammalian ODC is a homodimer with 2-fold symmetry. Each monomer has two domains: a β/α-barrel domain and a β-sheet domain.[13−16] The dimer contains two active sites, each of which is at the interface between a domain of one monomer and a subunit of the other;[12,14] the shared nature of the active sites means that the monomer has no activity. In PDB structure 1F3T, the monomers have molecular weight of about 47 kDa and contain 425 amino acids.[8] The catalytic mechanism of ODC is presented in Figure 1 and is typical for all PLP-dependent decarboxylases.[8,15,17]

The ornithine substrate (S) reacts with the enzyme-bond cofactor (PLP) via transaldimination reaction to form an external aldimine. In the subsequent step, the C_α−carboxylate bond is cleaved, releasing CO_2, and a quinonoid intermediate is formed. Protonation at Cα again forms an external aldimine, now consisting of putrescine (P) and PLP bound to each others via a Schiff-base linkage (PLP·P). In the next step putrescine is released, and the PLP−enzyme Schiff-base (E·PLP) internal aldimine is reformed, completing the catalytic cycle.

In the case of decarboxylation of ornithine by wild-type ODC, the observed carbon isotope effect, for C-13 substitution at the carboxyl carbon, is 1.033 at pH 7.3, whereas for the lysine and E274A cases, the observed carbon isotope effects are 1.063 and 1.055, respectively.[7] Using the latter results to infer that the intrinsic ^{13}C KIE for the wild-type enzyme with physiological substrate is close to 1.06, these experiments were used to infer that the commitment coefficient for this reaction is close to unity and that not only decarboxylation but also the rate of Schiff-base interchange is rate-limiting. The present investigation presents theoretical modeling that tests this interpretation. In particular, we calculate the intrinsic ^{13}C KIE on the decarboxylation of the ornithine−PLP and lysine−PLP Schiff bases to

(4) (a) O'Leary, M. H. *Annu. Rev. Biochem.* **1989**, *58*, 377. (b) Cleland, W. W. *CRC Crit. Rev. Biochem*. **1982**, *13*, 385. (c) Cleland, W. W. *Bioorg. Chem*. **1987**, *15*, 283. (d) Cook, P. F., Ed. *Enzyme Mechanisms from Isotope Effects*; CRC Press: Boca Raton, FL, 1991.
(5) Smiley, J. A.; Paneth, P.; O'Leary, M. H.; Bell, J. B.; Jones, M. E. *Biochemistry* **1991**, *30*, 6216.
(6) (a) Hermes, J. D.; Tipton, P. A.; Fisher, M. A.; O'Leary, M. H.; Morrison, J. F.; Cleland, W. W. *Biochemistry* **1984**, *23*, 6263. (b) Weiss, P. M.; Chen, C. Y.; Cleland, W. W.; Cook, P. F. *Biochemistry* **1988**, *27*, 4814. (c) Parmentier, L. E.; Smith, K. *J. Biochim. Biophys. Acta* **1998**, *1382*, 333. (d) Merkler, D. J.; Kline, P. C.; Weiss, P.; Schramm, V. L. *Biochemistry* **1993**, *32*, 12993. (e) Urbauer, J. L.; Bradshaw, D. E.; Cleland, W. W. *Biochemistry* **1998**, *37*, 18026. (f) Pawlak, J.; O'Leary, M. H.; Paneth, P. *J. Mol. Struct. THEOCHEM* **1998**, *454*, 69. (g) Drohat, A. C.; Jagadeesh, J.; Ferguson, E.; Stivers, J. T. *Biochemistry* **1999**, *38*, 11866. (h) Schramm, V. L. *Methods Enzymol*. **1999**, *308*, 301. (i) Bruner, M.; Horenstein, B. A. *Biochemistry* **2000**, *39*, 2261. (j) Yang, J.; Schenkman, S.; Horenstein, B. A. *Biochemistry* **2000**, *39*, 5902. (k) Gerratana, B.; Frey, P. A.; Cleland, W. W. *Biochemistry* **2001**, *40*, 2972. (l) Lewandowicz, A.; Rudzinski, J.; Tronstad, L.; Widersten, M.; Ryberg, P.; Patsson, O.; Paneth, P. *J. Am. Chem. Soc*. **2001**, *123*, 4550. (m) Snider, M. J.; Reinhardt, L.; Wolfenden, R.; Cleland, W. W. *Biochemistry* **2002**, *41*, 415. (n) Zheng, R.; Blanchard, J. S. *Biochemistry* **2003**, *42*, 11289. (o) Paneth, P. *Acc. Chem. Res*. **2003**, *36*, 120.
(7) Swanson, T.; Brooks, H. B.; Osterman, A. L.; O'Leary, M. H.; Phillips, M. A. *Biochemistry* **1998**, *37*, 14943.
(8) Jackson, L. K.; Brooks, H. B.; Osterman, A. L.; Goldsmith, E. J.; Phillips, M. A. *Biochemistry* **2000**, *39*, 11247.
(9) Osterman, A. L.; Kinch, L. N.; Grishin, N. V.; Phillips, M. A. *J. Biol. Chem*. **1995**, *270*, 11797.
(10) Pegg, A. E.; McGill, S. *Biochim. Biophys. Acta* **1979**, *568*, 416.
(11) (a) Seely, J. E.; Pösö, H.; Pegg, A. E. *Biochemistry* **1982**, *21*, 3394. (b) Coleman, C. S.; Stanley, B. A.; Pegg, A. E. *J. Biol. Chem*. **1993**, *268*, 24572. (c) Osterman, A.; Grishin, N. V.; Kinch, L. N.; Phillips, M. A. *Biochemistry* **1994**, *33*, 13662.
(12) Coleman, C. S.; Stanley, B. A.; Viswanath, R.; Pegg, A. E. *J. Biol. Chem*. **1994**, *269*, 3155.
(13) Osterman, A. L.; Kinch, L. N.; Grishin, N. V.; Phillips, M. A. *Biochemistry* **1995**, *34*, 13431.
(14) Tobias, K. E.; Kahana, C. *Biochemistry* **1993**, *32*, 5842.
(15) Kern, A. D.; Oliveira, M. A.; Coffino, P.; Hackert, M. L. *Structure Fold Des*. **1999**, *7*, 567.
(16) Almrud, J. J.; Oliveira, M. A.; Kern, A. D.; Grishin, N. V.; Phillips, M. A.; Hackert, M. L. *J. Mol. Biol*. **2000**, *295*, 7.
(17) Grishin, N. V.; Osterman, A. L.; Brooks, H. B.; Phillips, M. A.; Goldsmith, E. J. *Biochemistry* **1999**, *38*, 15174.

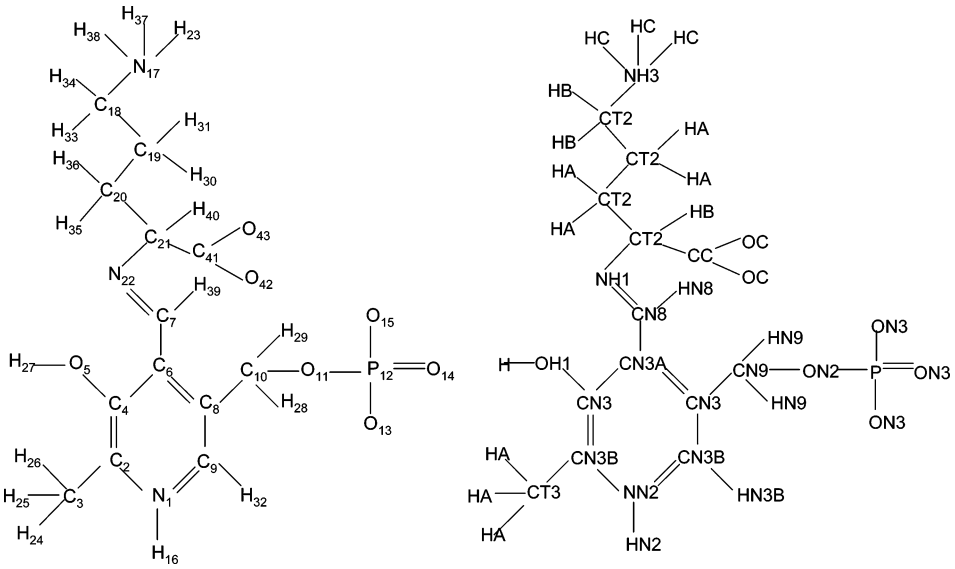

Figure 2. Atom numbering (left) and atom types (right) of the substrate−PLP Schiff-base models.

product−PLP Schiff bases and carbon dioxide for wild-type and mutant ODC. We show that for ODC the intrinsic ^{13}C KIE for wild-type enzyme and physiological substrate is significantly different from those for the slow substrate and the mutated enzyme.

Computational Methods

We used a combined quantum mechanical and molecular mechanical molecular dynamics (QM/MM/MD)[18] approach to study the decarboxylation step in ornithine decarboxylase catalysis. The QM part was described at the semiempirical level using the AM1 Hamiltonian,[19] and the MM part was based on the CHARMM22 all-atom force field.[20,21] The dynamics methodology has been reviewed recently,[22] and thus only a brief description with emphasis on aspects specific to the current calculations is presented here.

We have modeled three decarboxylation reactions catalyzed by ODC. The first model, which we label WEO (for *w*ild-type *e*nzyme with *o*rnithine), was used in studies of decarboxylation of ornithine in the active site of the wild-type enzyme. Analogously, the other two models correspond to decarboxylation of ornithine catalyzed by the E274A mutated enzyme, MEO, and decarboxylation of lysine catalyzed by wild-type enzyme, WEL. The core part of these models has been prepared on the basis of the available crystal structure[8] of ODC, complexed with the product and cofactor PLP, deposited in the Protein Data Bank (1F3T). This structure includes both monomers of the ODC homodimer, although 91 residues are missing. The remaining 759 residues were all included. In the case of the WEO and WEL models, atoms of the product in 1F3T have been replaced with atoms of the physiological substrate, ornithine, or the slow substrate, lysine, respectively. Model MEO is based on WEO with additional modification corresponding to E274A mutation.

To carry out MM optimizations and MD calculations on the whole system it is necessary to describe all atoms of the models in the CHARMM formalism. Standard CHARMM[20,21] topology and parameter files do not contain information regarding the PLP moiety or the amino acid L-ornithine; thus these data had to be provided externally. We described part of PLP using the existing atom types of nicotinic acid, and valence and van der Waals parameters of L-lysine were used for the homologous L-ornithine as illustrated in Figure 2, which also provides atom numbering for models WEO and MEO. (The partial charges for ornithine were obtained as discussed below.) All data regarding additional CHARMM parameters are given in the Supporting Information. Throughout this contribution we refer to this substrate−PLP Schiff-base moiety as the complex.

As indicated in Figure 1 the complex between PLP and the substrate does not have any covalent links with enzyme. Thus this complex, consisting of 43 atoms (46 in case of lysine), has been chosen to be treated at the quantum level in QM/MM formalism. The complex was optimized using the Hartree−Fock (HF) method with the 6-31G(d) basis set[23] implemented in *Gaussian98*.[24] Partial Mulliken charges from these calculations were used in the CHARMM force field. To test the reasonableness of the assigned atom types and partial charges, the gas-phase complex was optimized using CHARMM with the adopted basis Newton−Raphson (ABNR)[20] method with the default convergence criterion in the RMSD gradient, and good agreement with the HF/6-31G(d) structure was obtained.

This structure of the complex was inserted into the 1F3T structure of the enzyme. Then hydrogen atoms for the protein residues and crystallographic waters were added using the HBUILD module of CHARMM. Then, the system was minimized for 100 steps using the ABNR method of CHARMM. To include the effect of the solvent, a 30 Å sphere of TIP3P[25] equilibrated water molecules was added. The origin of this sphere was placed at the reaction center, which is defined as the geometric center of the $C_{21}-C_{41}$ bond, where C_{21} is the α-carbon of the Schiff base, and C_{41} is the carbon of the carboxyl group (see Figure 2). Figure 3 shows clearly that the water sphere centered at one of the active sites does not include most of the second monomer

(18) (a) Field, M. J.; Bash, P. A.; Karplus, M. *J. Comput. Chem.* **1990**, *11*, 700. (b) Gao, J. In *Reviews in Computational Chemistry*; Lipkowitz, K. B., Boyd, D. B., Eds.; VCH: New York, 1996; Volume 7, p 119. (c) Gao, J., Thompson, M. A., Eds.; *Combined Quantum Mechanical and Molecular Mechanical Methods*; American Chemical Society: Washington, DC, 1998; p 712. (d) Amara, P.; Field, M. J. In *Computational Molecular Biology*; Leszczynski, J., Ed.; Elsevier: Amsterdam, 1999; p 1. (e) Gao, J.; Truhlar, D. G. *Annu. Rev. Phys. Chem.* **2002**, *53*, 467.
(19) (a) Dewar, M. J. S.; Zoebisch, E. G.; Healy, E. F.; Stewart, J. J. P. *J. Am. Chem. Soc.* **1985**, *107*, 3902. (b) Dewar, M. J. S.; Jie, C.; Yu, G. *Tetrahedron* **1993**, *23*, 5003. (c) Holder, A. J.; Dennington, R. D.; Jie, C.; Yu, G. *Tetrahedron* **1994**, *50*, 627.
(20) Brooks, B. R.; Bruccoleri, R. E.; Olafson, B. D.; States, D. J.; Swaminathan, S.; Karplus, M. *J. Comput. Chem.* **1983**, *4*, 187.
(21) (a) Reiher, W. E., II. Theoretical Studies of Hydrogen Bonding. Ph.D. Thesis, Harvard University, Cambridge, MA, 1985. (b) MacKerell, A. D., Jr.; et al. *J. Phys. Chem. B* **1998**, *102*, 3586.
(22) Truhlar, D. G.; Gao, J.; Garcia-Viloca, M.; Alhambra, C.; Corchado, J.; Sanchez, M. L.; Poulson, T. D. *Int. J. Quantum Chem.* **2004**, *100*, 1136.
(23) (a) Hariharan, P. C.; Pople, J. A. *Theor. Chim. Acta* **1973**, *28*, 213. (b) Francl, M. M.; Pietro, W. J.; Hehre, W. J.; Binkley, J. S.; Gordon, M. S.; DeFrees, D. J.; Pople, J. A. *J. Chem. Phys.* **1982**, *77*, 3654.
(24) Frisch, M. J.; et al. *Gaussian 98*, revision A.11; Gaussian, Inc.: Pittsburgh, PA, 1998.
(25) Jorgensen, W. L.; Chandrasekhar, J.; Madura, J. D.; Impey, R. W.; Klein, M. L. *J. Chem. Phys.* **1983**, *79*, 926.

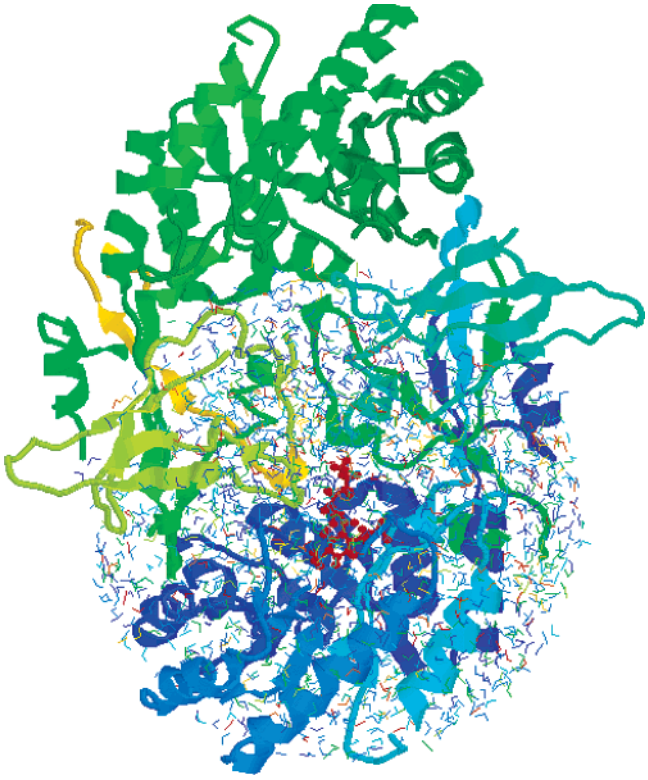

Figure 3. Enzyme model set WEO for the QM/MM calculation. The water molecules are shown as sticks, the protein is represented by cartoons, and the substrate−PLP complex is depicted in red.

of the homodimer. Water molecules at a distance less than 2.5 Å from any protein atom or crystallographic waters were removed.

In the next step, all the waters present in the system were subjected to 500 cycles of geometry optimization using ABNR method. In these calculations the active site and the protein atoms were kept frozen. Any water molecule that happened to move outside the 30 Å sphere was deleted. Then the geometry of the protein along with complex was optimized with water atoms kept frozen. Then the system was divided into the QM and MM parts for the purpose of calculating the potential energy surface and forces. The QM subsystem consisted of 43 or 46 atoms including the PLP molecule and ornithine (WEO, MEO) or lysine (WEL), respectively. The total charge of the QM part was −1, while the total charge on the whole models was +5. The models consisted of 759 backbone amino acids, 1986, 1990, or 1980 water molecules (depending on the model), the substrate, and PLP, resulting in a total of 17 883, 17 898, and 17 857 atoms for WEO, MEO, and WEL, respectively. Figure 3 illustrates the final model for WEO.

The remaining steps of the calculational protocol followed strictly the single-reaction-coordinate part of the published scenario[22] with the only difference that the reaction coordinate z was defined as a single interatomic distance:

$$z = r(C_{21} - C_{41}) \tag{3}$$

rather than a combination of two bond distances.

Prior to the molecular dynamics calculation the whole system within the 30 Å sphere was subjected to 500 cycles of the ABNR minimization to relax any possible bad contacts in the initial positions of the crystal structure. Then the molecular dynamics calculations were performed for 5 ps on water molecules within a 25 Å sphere around the reactive center. During this period the temperature was increased from 60 to 80 K.

The classical potential of mean force[26] (PMF) on the reaction coordinate z was computed to account for the ensemble of different conformations of generalized transition state species along the reaction coordinate. The PMF was determined with the use of stochastic boundary molecular dynamics method[27] (SBMD); this involves partitioning the system into three regions. The reaction region has unrestrained molecular dynamics and contains the substrate, cofactor, and residues and water molecules for which any atom is within 25 Å of the reaction center. This includes 8268 (WEO), 8225 (WEL), or 8235 (MEO) atoms. The atoms belonging to residues and water molecules lying outside the reaction region but within a 30 Å radius constitute the buffer region, which is treated as a heat bath with Langevin dynamics.[27] The buffer regions contains 4731 (WEO), 4691 (WEL), or 4659 (MEO) atoms. All other atoms of the protein were treated as a reservoir region that provides a static force field and were kept frozen in the dynamics calculations. The reservoir region contains 4884 (WEO), 4982 (WEL), or 4963 (MEO) atoms. In the buffer region, friction coefficients of 200 ps^{-1} for protein atoms and 62 ps^{-1} for water atoms were used, as in previous[28−31] work. A leapfrog algorithm was used with an integration time step of 1 fs in all the calculations. Nonbonded cutoffs of 13 Å based on the center-of-mass separation of the interacting groups were chosen for both QM/MM and MM interactions. During the SBMD simulation all the bonds involving the hydrogen atoms except those of the QM subsystem were constrained to their equilibrium distances using the SHAKE algorithm.[32] Then, over 30 ps, the system was gradually heated to the final temperature of 298 K. Every 5 steps of simulation the temperature was increased by 5 K during the heating stage. After that it was equilibrated for 50 ps. All the rest of the calculations were performed at a temperature T of 298 K.

The classical PMF, denoted $W(T,z)$, was calculated by combining the QM/MM force field, the SBMD dynamics scheme, and the umbrella sampling[28,30,31,33,34] technique. The simulations were carried out in 11 overlapping windows, each 0.2 Å wide, to cover the entire reaction coordinate. For each window, we carried out 20 ps of equilibration and 50 ps of ensemble averaging. The results were sorted into bins of width 0.01 Å, yielding the curves shown in Figure 4. The bin with the highest PMF is the classical mechanical variational transition state. This bin occurred at $z = 2.12$, 2.15, and 2.20 Å for WEO, WEL, and MEO, respectively.

In the next step, the PMF was quantized. These calculations were carried out using the CHARMMRATE module[35] of CHARMM[20], based on the interface of CHARMM and POLYRATE.[36] This step requires the partition into a primary zone and a secondary zone,[30,31] and we used the same partition as for the QM/MM partition; this results in 43 or 46 atoms in the primary zone and the rest in the secondary zone. The quantized PMF equals the classical PMF of the entire system plus the average of the difference between the quantized and classical vibrational free energy of the primary zone.[31,34] This difference was calculated by generalized normal-mode analysis with projected numer-

(26) Hill, T. L. *An Introduction to Statistical Thermodynamics*; Addition-Wesley: Reading, MA, 1960; p 313.
(27) Brooks, S. L., III; Brünger, A.; Karplus, M. *Biopolymers* **1985**, *24*, 843.
(28) Alhambra, C.; Wu, L.; Zhang, Z.-Y.; Gao, J. *J. Am. Chem. Soc*. **1998**, *120*, 3858.
(29) Alhambra, C.; Gao, J. *J. Comput. Chem*. **2000**, *21*, 1192.
(30) (a) Alhambra, C.; Gao, J.; Corchado, J. C.; Sanchez, M. L.; Truhlar, D. G. *J. Am. Chem. Soc*. **2000**, *122*, 8197. (b) Alhambra, C.; Gao, J.; Corchado, J. C.; Sanchez, M. L.; Garcia-Viloca, M.; Truhlar, D. G. *J. Phys. Chem. B* **2001**, *105*, 11326. (c) Alhambra, C.; Sanchez, M. L.; Corchado, J.; Gao, J.; Truhlar, D. G. *Chem. Phys. Lett*. **2001**, *347*, 512; **2002**, *355*, 388(E).
(31) Garcia-Viloca, M.; Alhambra, C.; Truhlar, D. G.; Gao, J. *J. Comput. Chem*. **2003**, *24*, 177.
(32) Ryckaert, J. P.; Cicotti, G.; Berendsen, H. J. C. *J. Comput. Chem*. **1977**, *23*, 327.
(33) (a) Valleau, J. P.; Torrie, G. M. *Statistical Mechanics*; Berne, B. J., Ed.; Plenum: New York, 1977; Part A, p 137. (b) Torrie, G. M.; Valleau, J. P. *J. Chem. Phys*. **1977**, *23*, 187. (c) Kottalam, J.; Case, D. A. *J. Am. Chem. Soc*. **1988**, *110*, 7690. (d) Roux, B. *Comput. Phys. Commun*. **1995**, *91*, 275. (e) Alhambra, C.; Wu, L.; Zhang, Z.-Y.; Gao, J. *J. Am. Chem. Soc*. **1998**, *120*, 3858.
(34) Garcia-Viloca, M.; Alhambra, C.; Truhlar, D. G.; Gao, J. *J. Chem. Phys*. **2001**, *114*, 9953.
(35) Alhambra, C.; Corchado, J. C.; Sánchez, M. L.; Villà, J.; Gao, J.; Truhlar, D. G. *CHARMMRATE*, version 1.0; University of Minnesota: Minneapolis, 1999.

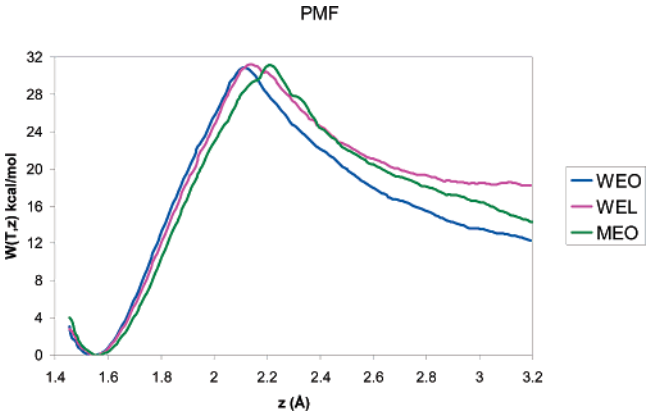

Figure 4. Classical mechanical PMFs for WEO, WEL, and MEO as functions of the reaction coordinate.

ical Hessians in rectilinear coordinates for 250 configurations each in the windows corresponding to reactant, classical variational transition state, and product, respectively. These 750 samples were sorted into bins of width 0.01 Å, and the results were averaged in each bin. The resulting averages were fit to a fifth-order (WEO) or third-order (WEL and MEO) polynomial as a function of z, where z is the center of the bin, and the polynomial was added to the classical PMF to produce the quasiclassical PMF, denoted $W^{QC}(T,z)$. The quantization step was then repeated with C-13 substituted for C-12 at C_{41}. The minima of these curves define the reactant ensembles, and the maxima of the quasiclassical PMFs define the variational transition states, denoted by $z = z_*$. These maxima were found to occur at the same value of z for C-12 and C-13, and in particular at the same locations as the maxima of the classical PMFs, that is, at $z = 2.12$ Å for WEO, 2.15 Å for WEL, and 2.20 Å for MEO.

The quasiclassical free energy of activation profile $\Delta G_T^{(1)}(z)$ was computed from the quasiclassical PMF by the method of ref 31. The maxima of $\Delta G_T^{(1)}(z)$ occur at the same locations as the maxima z_* of the quasiclassical PMFs, and the values at these locations are denoted $\Delta G_T^{\ddagger}$.

Results and Discussion

The maxima of the classical PMFs, the quasiclassical PMFs, and the free energy of activation profiles are all given in Table 1. The quasiclassical absolute rate constants for the chemical step for each isotopic species are then given by

$$k(T) = \frac{k_B T}{h} \exp(-\Delta G_T^{\ddagger}/RT) \qquad (4)$$

where k_B is Boltzmann's constant, h is Planck's constant, and R is the gas constant. This corresponds to Eyring theory,[37] as extended[22,38] to the condensed phase. In all three cases the reaction is endoergic as shown in Figure 4. Recrossing corrections were assumed to be unity, since previous studies indicate that they are close to unity[22,30,31,39,40] and not strongly dependent on an isotopic substitution.[30,31,40] Comparison of the calculated KIEs in Table 2 with the activation parameters in Table 1 shows that the calculated intrinsic ^{13}C KIEs correlate with values of the activation barriers; the largest barriers, which are found for the WEL and MEO models, correspond to the largest KIEs. The WEO reaction has a slightly smaller activation barrier and a substantially smaller ^{13}C KIE. In general, one would want to be cautious about interpreting activation parameter changes as small as 0.4 kcal/mol, but it is encouraging that the differences are systematic in the present case.

Table 1. Transition State Activation Parameters[a]

quantity	WEO	WEL	MEO
max $W(T,z)$	31.09	31.50	31.46
$W^{QC}(T,z_*)$: C-12	30.83	31.24	31.20
C-13	30.86	31.24	31.23
$\Delta G_T^{\ddagger}$: C-12	30.33	30.46	30.52
C-13	30.36	30.50	30.56

[a] Relative to reactants.

Table 2. Experimental and Calculated Intrinsic ^{13}C KIEs for ODC Reactions

model	WEO	WEL	MEO
calculated KIE_5	1.041	1.059	1.058
KIE_{obsd}[a]	1.033	1.063	1.055

[a] The experimentalists' error bars are less than 1 in the last digit tabulated.

Table 2 shows that carbon kinetic isotope effects on the decarboxylation reaction for the native ODC with slow substrate (WEL), as well as for the mutant enzyme (MEO), are of similar size and close to 1.06. Table 2 also compares to experiment. However, this comparison is not a strict one because Table 2 compares calculated KIEs for step 5 within the enzyme active site to observed KIEs for the enzymatic reaction defined such that the reactants are the free substrate in solution. The comparison of theory to experiment can be interpreted quantitatively only in the absence of any equilibrium isotope effect (EIE) for formation of the reactant complex for step 5, and we have no information on that. However, the agreement between theory and experiment is consistent with that EIE being close to unity. Furthermore, the agreement between the experimentally observed values and the predicted intrinsic ^{13}C KIEs for these models suggests that in both cases the decarboxylation step is solely rate-determining, and the intrinsic value is almost fully expressed in the experimentally observed KIEs. These results fit nicely into the current thinking about enzymatic decarboxylations, for which intrinsic ^{13}C KIEs in the range of 1.05−1.06 are expected.[2] (Values in this range are also found for nonenzymatic decarboxylations.[41]) Within this framework the much smaller value observed for the physiological substrate (1.033) was interpreted as evidence that an isotopically insensitive step precedes the decarboxylation and is partially rate-limiting; in terms of eqs 1 and 2 this would mean that the commitment to

(36) (a) Chuang, Y.-Y.; Corchado, J. C.; Fast, P. L.; Villà, J.; Hu, W.-P.; Liu, Y.-P.; Lynch, G. C.; Jackels, C. F.; Nguyen, K. A.; Gu, M. Z.; Rossi, I.; Coitiño, E. L.; Clayton, S.; Melisss, V. S.; Lynch, B. J.; Fernandez-Ramos, A.; Pu, J.; Stecker, R. B.; Garrett, C.; Isaacson, A. D.; Truhlar, D. G. *POLYRATE*, version 8.7.2; University of Minnesota: Minneapolis, 2002. (b) Chuang, Y.-Y.; Corchado, J. C.; Fast, P. L.; Villà, J.; Hu, W.-P.; Liu, Y.-P.; Lynch, G. C.; Jackels, C. F.; Nguyen, K. A.; Gu, M. Z.; Rossi, I.; Coitiño, E. L.; Clayton, S.; Melissas, V. S.; Lynch, B. J.; Fernandez-Ramos, A.; Pu, J.; Albu, T.; Steckler, R. B.; Garrett, C.; Isaacson, A. D.; Truhlar, D. G. *POLYRATE*, version 9.0; University of Minnesota: Minneapolis, 2002.
(37) (a) Glasstone, S.; Laidler, K. J.; Eyring, H. *The Theory of Rate Processes*; McGraw-Hill: New York, 1941. (b) Johnson, F. H.; Eyring, H.; Stover, B. J. *The Theory of Rate Process in Biology and Medicine*; Wiley & Sons: New York, 1974.
(38) Truhlar, D. G. In *Isotope Effects in Chemistry and Biology*; Limbach, H., Kohen, A., Eds.; Marcel Dekker: New York, 2005; in press.
(39) (a) Neria, E.; Karplus, M. *Chem. Phys. Lett.* **1997**, *267*, 23. (b) Villa, J.; Warshel, A. *J. Phys. Chem. B* **2001**, *105*, 7887. (c) Nam, K.; Prat-Resina, X.; Garcia-Viloca, M.; Devi-Kesavan, L. S.; Gao, J. *J. Am. Chem. Soc.* **2004**, *126*, 1369.
(40) Agrawal, P. K.; Billeter, S. R.; Hammes-Schiffer, S. *J. Phys. Chem. B* **2002**, *106*, 3283.
(41) Sicinska, D.; Truhlar, D. G.; Paneth, P. *J. Am. Chem. Soc.* **2001**, *123*, 7683.

Table 3. Geometric Parameters of the Transition States of Studied Models

	WEO	WEL	MEO
	Bonds (Å)[a]		
$C_{21}-C_{41}$	2.12[0.61][b]	2.15[0.62]	2.20[0.66]
$C_{21}-N_{22}$	1.38[−0.09]	1.33[−0.13]	1.34[−0.09]
$N_{22}-C_7$	1.30[0.02]	1.32[0.04]	1.33[0.05]
C_7-C_6	1.46[−0.06]	1.42[−0.08]	1.43[−0.06]
N_1-C_2	1.34[−0.04]	1.37[−0.01]	1.37[−0.04]
$C_{41}-O_{42}$	1.23[−0.04]	1.22[−0.07]	1.22[−0.07]
$C_{41}-O_{43}$	1.21[−0.05]	1.21[−0.08]	1.20[−0.04]
	Valence Angle		
$O_{42}-C_{41}-O_{43}$	151.5[28.1]	149.4[33.1]	152.4[33.2]
	Dihedral Angles		
$N_{22}-C_{21}-C_{41}-O_{43}$	70.9(45.6)[c]	114.0(135.0)	74.0(78.7)
$C_7-N_{22}-C_{21}-C_{41}$	−81.7(20.5)	−97.5(−117.0)	108.6(18.6)
C4−C6−C_7-N_{22}	35.5(−106.5)	13.5(26.3)	−42.8(−72.7)

[a] Numbering given in Figure 2. [b] Values in brackets give changes from substrate to TS; a minus sign indicates shortening of a bond. [c] Values in parentheses give values for the substrate.

catalysis C is close to unity.[42] Although it is not essential to our key points, we note that for the present case of a mechanism (Figure 1, where the intrinsic isotope effect is connected with the rate constant k_5) more complicated than the one illustrated by eq 1, the mathematical expression for the commitment is different and is given by $C = k_5/k_4(1 + k_3/k_2)$.

The most important finding of this study is a substantial difference between the intrinsic KIEs for physiological substrate and slow substrate. The calculated value of ^{13}C KIE for the chemical step of the decarboxylation of ornithine catalyzed by ODC is only 1.04. This means that, at least in the present example of ODC-catalyzed decarboxylation, ^{13}C KIE obtained for the slow substrate (or mutated enzyme) *cannot* be considered as a model for the intrinsic ^{13}C KIE for the reaction of physiological substrate catalyzed by the wild-type enzyme. Comparison of the theoretically predicted intrinsic ^{13}C KIE for the physiological substrate and the wild-type enzyme indicates that the commitment C is small and that the chemical decarboxylation step is also mostly rate-determining in this case for competitively measured KIEs that probe steps through the first irreversible step. In fact, assuming unity for the EIE, eq 2 yields $C = 0.24$. Thus, from the mechanistic point of view, this means that the transition state structures for the decarboxylations of physiological and slow substrates, as well as those for the wild-type and mutated enzymes, are significantly different. To elucidate the origins of these differences, we have performed detailed analyses of the transition states of the three systems under study.

Table 3 lists geometrical parameters of the transition states that change substantially on going from the substrates to transition states, or are substantially different between the three reactions. (The values in Table 3 were averaged over the same 250 free-energy-selected nonstationary structures as those used to compute the quantized vibrational energy at the transition state.) The top part of the table lists bond distances together with their change from substrate, with the latter given in brackets. Negative values in the brackets correspond to the shortening of a bond. The most prominent differences are exhibited in the $C_{21}-C_{41}$ bond length, which is the reaction coordinate. For all three models this bond is elongated by more than 0.6 Å as compared to the corresponding substrate−PLP complexes; by Pauling's relation,[43] this would correspond to a decrease in bond order from 1.00 to 0.10 (which means that the bond is far more than half broken), and therefore we conclude that all three complexes are late transition states. (However, see below for a different conclusion based on bond angles.) The shortest value of 2.12 Å is observed for the WEO model. This is paralleled by shorter $N_{22}-C_7$ and N_1-C_2 bonds and longer $C_{21}-N_{22}$ and C_7-C_6 bonds as compared to the other two models, which have these bonds altered more toward the quinonoid character of the complex of PLP with the product. These geometrical features place the transition state of the WEO model at the earliest position along the reaction coordinate. Interestingly, the C−O bond distances of the carboxyl groups do not show noticeable variations between the transition state models. Among all the other valence coordinates the only substantial change on going from the substrates to the TSs is observed for the $O_{42}-C_{41}-O_{43}$ bond angle of the carboxyl groups, although the spread is very small. In all three models this angle is close to 150°, which is the mean of 120° characteristic for the sp^2 hybridization of the reactant carboxyl carbon and 180° characteristic of the sp carbon in the product CO_2, suggesting that all TSs are midway between reactants and products in terms of this bond angle.

The largest differences between the three models are found in the dihedral angles. Figures 5 and 6 show the orientation of the QM parts of the models. To discuss the spatial features of the models we use a convention where the aromatic ring is oriented as in Figure 1, in which methyl and hydroxyl substituents are on the left side of the ring. We use this convention in all of the figures in this contribution except Figure 6. Transition states in Figures 5 and 6 are rendered in green and are superimposed over the corresponding substrate−PLP complexes. Several differences between the models are noteworthy.

In gas-phase transition state theory, if one makes the assumption that the transition state structure is at the saddle point and hence independent of isotopic substitution, the high-temperature limit of the C-12/C-13 kinetic isotope effect (aside from symmetry factors) is $\omega^{\ddagger}_{C-12}/\omega^{\ddagger}_{C-13}$ where $\omega^{\ddagger}$ is the imaginary frequency.[44] This quantity, sometimes called the temperature-independent factor, is useful even at finite temperature because it provides a measure of isotopic movement in the reaction-coordinate motion. To gain insight into the present reaction, we performed a more detailed analysis of 10 representative transition state configurations (for each model) obtained by free-energy-based sampling. (This means, in the present context, that configurations are sampled by a scheme where geometries that are equally likely to be occupied at equilibrium are selected with equal probability, and hence the sample points are appropriately averaged with equal weight.) In particular, 10 bath configurations were chosen in the bin corresponding to $z_* \pm 0.005$ Å. For each configuration, the primary zone was optimized to the nearest saddle point in the field of a fixed secondary zone. Then we performed normal-

(42) (a) Cook, P. F.; Cleland, W. W. *Biochemistry* **1981**, *20*, 1790. (b) Hermes, J. D.; Roeske, C. A.; O'Leary, M. M.; Cleland, W. W. *Biochemistry* **1982**, *21*, 5106. (c) Paneth, P. In *Heavy Atom Isotope Effects*; Buncel, E., Saunders, W. H., Jr., Eds.; Isotopes in Organic Chemistry; Elsevier: Amsterdam, 1992; Volume 8, p 41.

(43) Pauling, L. *J. Am. Chem. Soc.* **1947**, *69*, 542.

(44) Melander, L.; Saunders, W. H., Jr. *Reaction Rates of Isotopic Molecules*; Wiley: New York, 1980.

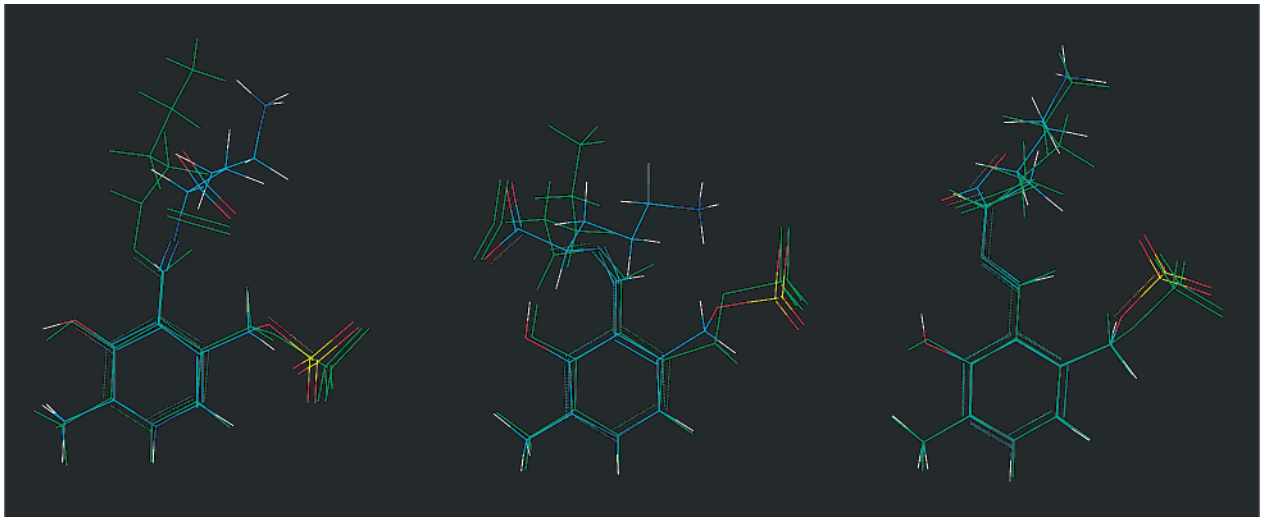

Figure 5. Structures of the QM models, from left to right: WEO, WEL, and MEO. Transition states (rendered in green) are superimposed over the corresponding substrate−PLP complexes.

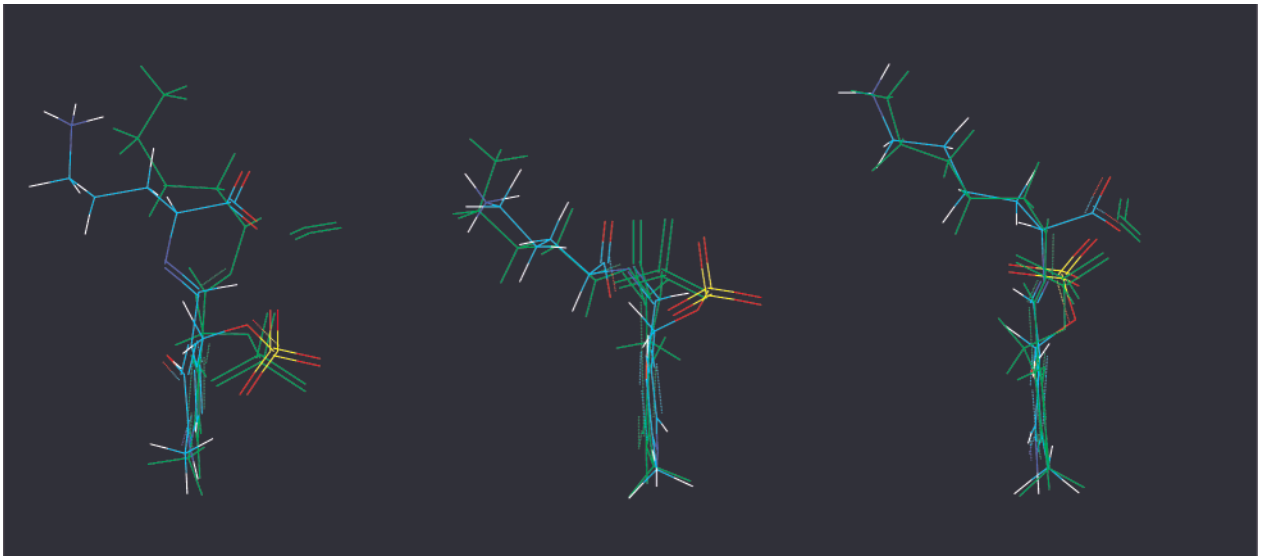

Figure 6. Side view of the QM models (with phosphate groups directed behind the plane). From left to right: WEO, WEL, and MEO. Transition states (rendered in green) are superimposed over the corresponding substrate−PLP complexes.

Table 4. Imaginary Frequencies (cm^{-1}) and Their Ratios

quantity	WEO	WEL	MEO
$\omega^{\ddagger}_{C-12}$	475.7i	501.6i	376.6i
$\omega^{\ddagger}_{C-13}$	465.5i	490.3i	367.7i
$\omega^{\ddagger}_{C-12}/\omega^{\ddagger}_{C-13}$	1.022	1.023	1.024

mode analysis at these saddle points and averaged the resulting imaginary frequencies. The results are given in Table 4. The temperature-independent factors are very similar for all three reactions. This fact will be critical for the argument in the next paragraph.

Both substrates extend behind the aromatic ring. For the WEO and MEO models, the carboxylic group is directed toward the front of the ring plane while ornithine is directed behind this plane in the ornithine−PLP complexes. The extended length of lysine (WEL model) forces the carboxyl group closer to the plane of the ring so that CO_2 is expelled to the right (in the orientation of Figure 5) rather than to the front of the ring. This is reflected in the similar values of the $N_{22}-C_{21}-C_{41}-O_{43}$ dihedral for WEO and MEO and a different value for WEL (see Table 3). The main differences between the three models are associated with the central $C_7-N_{22}-C_{21}$ fragment. As evidenced by the $C_4-C_6-C_7-N_{22}$ dihedrals in the WEL and MEO models, there is little movement of this fragment in going from the substrate to the transition state, although the position of N_{22} is behind the ring plane in MEO and close to ring plane in WEL (again due to the effect of the longer substrate that is too long to fit comfortably in the active site). Unlike the other two cases, in the case of WEO the $C_7-N_{22}-C_{21}$ fragment moves a considerable distance as the system progresses along the reaction coordinate. As a result, N_{22}, which is behind the ring plane in the substrate, moves in front of this plane in the transition state. The fact that the temperature-independent factors for all three models are very close (Table 4) suggests that coupling of this ornithine movement to the reaction coordinate is not the source of the noticeably smaller intrinsic ^{13}C KIE in the case of WEO. Thus, the difference must arise from a different environment around the isotopic atom. We have analyzed the changes in the surroundings of the isotopic atom

Table 5. Changes of AM1 Mulliken Partial Atomic Charges between TSs and Substrates

atom	WEO	WEL	MEO
sum on carboxyl group	0.73	0.63	0.86
C_{21}	0.10	0.09	0.09
N_{22}	0.10	0.09	0.05
C_7	−0.36	−0.24	−0.14
sum on aromatic ring and its substituents[a]	−0.81	−0.42	−0.96
sum on phosphate group[b]	0.02	−0.10	−0.11

[a] Includes whole groups bonded to the ring. [b] PO_4.

by calculating charge distributions and hydrogen bond distances in the active sites of the models.

Table 5 presents the changes in the AM1 Mulliken partial atomic charges on key atoms and groups between the transition states and the corresponding substrates for the three ODC models. Each set of charges is averaged over 10 configurations; we used the same 10 optimized structures as described above for the imaginary frequency calculations. We also optimized the primary-zone atoms of the reactant to local minima and calculated average charges for the reactant. The differences of the representative averages are in Table 5.

Since the product, carbon dioxide, is a neutral molecule and the carboxylic group bears a formal charge of −1 in the substrate−PLP Schiff base, one can expect that the absolute magnitude of this charge decreases as the transition state structure becomes more productlike. As can be seen from the first line of Table 5, most of the negative charge is lost from atoms of the departing carboxyl group (it is transferred into the PLP moiety). However, the extent of the charge transfer does not parallel the extent of the rupture of the dissociating bond, which indicates that some additional interactions are present in the active sites. A likely candidate for such a charge distribution disturbance is the hydrogen bond network.

As illustrated in Figure 7, the reacting complexes have two major hydrogen bond contacts within the active sites. One is with the departing CO_2 moiety, and the other is with the phosphate group of PLP. In all three models, water molecule H_2O88 is present in the active site and makes a hydrogen bond with one of the oxygen atoms of the phosphate group. Additionally, in the MEO transition state a N−H···O hydrogen bond between the amide hydrogen of phenylalanine F209 and oxygen O_{13} of the phosphate group of PLP is present (Table 6). In the WEL and MEO models, a hydrogen bond is formed between an oxygen atom of the carboxyl group and water molecule H_2O952 or the hydroxyl group of PLP, respectively. The WEO model differs from the other two in that both oxygen atoms of the carboxylic group are hydrogen bonded. The presence of two hydrogen bonds restricts movements of the carboxylic group; this is reflected in the shortest C_{21}−C_{41} bond length in the transition state and is most probably the reason for the smaller intrinsic carbon kinetic isotope effect for this reaction. Acceleration of reaction rates by increased number and/or strengths of hydrogen bonds at the transition states has been observed previously for reactions in aqueous solution[45] and in

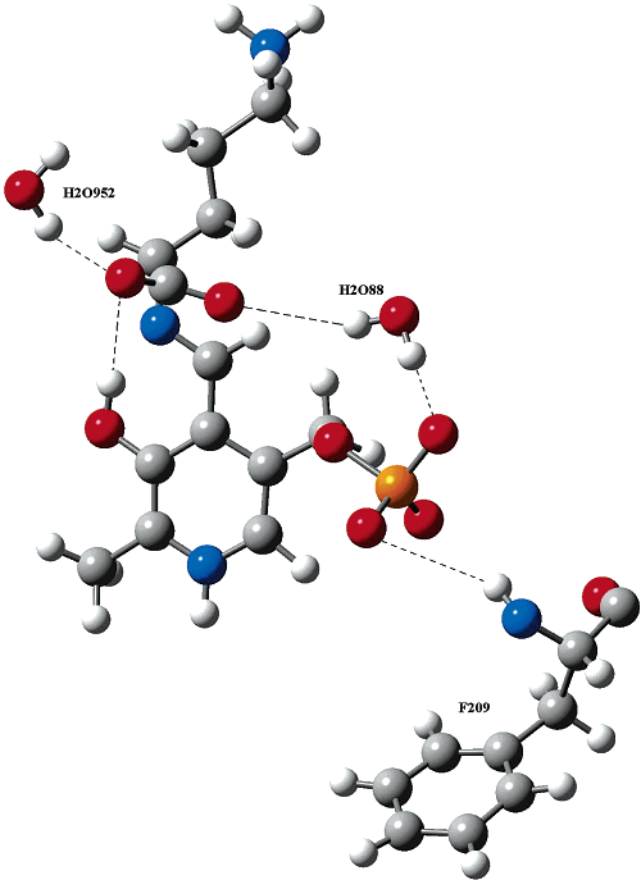

Figure 7. Hydrogen bond networks of the transition states with the active site residues.

enzymes,[46] and thus the effect of differential hydrogen bonding is well-known, but the present observations of a variable number of hydrogen bonds to the active atoms for two substrates of the same enzyme and for a wild-type and mutated enzyme are particularly striking.

The complexity of the competing factors influencing the transition state is illustrated by the nonsynchronous nature of the various progress variables, which was already noted above. For example, consideration of the C_{21}−C_{41} bond length puts the transition states in the order WEO (earliest) < WEL < MEO (latest), whereas considering charge transfer from CO_2 yields the order WEL (earliest) < WEO < MEO (latest). If one had attempted to predict these trends from the Hammond postulate[47] and the endoergodicities, one would have surmised WEO < MEO < WEL. The fact that the Hammond postulate fails for the C−C distance is illustrated by the crossing of the MEO and WEL PMFs in the exit valley in Figure 4. This kind of complexity in enzyme mechanisms is one reason enzyme simulations were unreliable until recent progress in combined QM/MM simulations allowed free-energy-based sampling of transition state structures,[30] as employed here. It is very encouraging that the above analysis not only uncovers a substrate dependence of the intrinsic KIE but also allows for a rational explanation of this dependence in terms of hydrogen bonding.

(45) (a) Severence, D. L.; Jorgensen, W. L. In *Structure and Reactivity in Aqueous Solution: Characterization of Chemical and Biological Systems*; Cramer, C. J., Truhlar, D. G., Eds.; ACS Symposium Series 568; American Chemical Society: Washington, DC, 1994; p 243. (b) Lim, D.; Jensen, C.; Repasky, M. P.; Jorgensen, W. L. In *Transition State Modeling for Catalysis*; Truhlar, D. G., Ed.; ACS Symposium Series 721; American Chemical Society: Washington, DC, 1999; p 74.

(46) (a) Alhambra, C.; Wu, L.; Zhang, Y.-Z.; Gao, J. *J. Am. Chem. Soc.* **1998**, *120*, 3858. (b) Garcia-Viloca, M.; Gao, J.; Karplus, M.; Truhlar, D. G. *Science* **2004**, *303*, 186.

(47) Hammond, G. S. *J. Am. Chem. Soc.* **1955**, *77*, 334.

Table 6. Hydrogen Bonds Lengths and O···H Distances in Hydrogen Bonds (Å) in the Active Sites[a]

active site moiety	structure	WEO $O_{42}/O_{43}/O_{15}$	WEL O_{42}/O_{15}	MEO O_{42}/O_{13}
H_2O952	substrate	−/2.90(1.96)/−	−	−
	transition state	−/2.69(1.88)/−		
H_2O88	substrate	2.81(1.88)/−/2.88(1.96)	3.05(2.13)/2.81(1.86)	−/2.86(2.09)
	transition state	3.11(2.31)/−/2.60(1.71)	2.85(2.01)/2.61(1.67)	−/2.80(2.26)
F209	substrate	−	−	−
	transition state			−/2.99(2.00)
PLP−O_5H_{27}	substrate	−	−	2.69(2.03)/−
	transition state			2.64(2.13)/−

[a] Averaged over the same structures, selected by free-energy-based sampling, that were used for Table 3. O···H distances are given in parentheses.

Conclusions

Two key results are presented here. First, from the mechanistic point of view, we show that the transition state for the wild-type ODC enzyme and physiological substrate (ornithine) is different (earlier and with one more hydrogen bond to the carboxyl group) from the transition state for the reaction of slow substrate (lysine) or the transition state of the mutated enzyme. Second, this difference in structure leads to a much smaller intrinsic carbon kinetic isotope effect for the physiological substrate. To the best of our knowledge, such a large difference in the intrinsic value for a heavy-atom KIE has never been documented in earlier work. Thus, our results serve as a warning that the commonly accepted method for interpreting carbon KIEs by using the observed KIE for a slow substrate as a model of the intrinsic value for the physiological substrate is not always safe, and it may lead to false conclusions regarding relative rate constants. The observed KIE for the wild-type enzyme with physiological substrate, together with the calculated intrinsic value of the KIE, yields a value of commitment to catalysis in this reaction of about 0.24. Thus, similarly to what was observed in the slow-substrate and mutated-enzyme cases, the rate of the whole enzymatic process is mostly limited by the decarboxylation step.

Acknowledgment. This work was supported by the grant from the State Committee for Scientific Research, Poland, and the National Science Foundation under Grant No. CHE03-49122. We thank Dr. Agnieszka Dybała-Defratyka for helpful discussions. Use of supercomputer facilities at MSI (Minneapolis), ICM (Warsaw), and PCSS (Poznan) are acknowledged.

Supporting Information Available: CHARMM topology and parameters specific to substrate−PLP complexes as well as complete refs 21b and 24. This material is available free of charge via the Internet at http://pubs.acs.org.

JA042298P